A Reaction-Induced FT-IR Study of Cyanobacterial Photosystem I†

Sunyoung Kim,‡,§ Colette A. Sacksteder,‡ Kathryn A. Bixby, and Bridgette A. Barry*

Department of Biochemistry, Molecular Biology, and Biophysics, University of Minnesota, St. Paul, Minnesota 55108-1022

Received May 18, 2001; Revised Manuscript Received October 11, 2001

ABSTRACT: In oxygenic photosynthesis, photosystem I (PSI) conducts light-driven electron transfer from plastocyanin to ferredoxin. The reactions are initiated when the primary chlorophyll donor, P_{700}, is photooxidized. P_{700} is a chlorophyll dimer ligated by the core subunits *psaA* and *psaB*. A difference Fourier transform infrared spectrum, associated with P_{700}^+-minus-P_{700}, can be acquired using PSI from the cyanobacterium *Synechocystis sp.* PCC 6803. This spectrum reflects contributions from oxidation-sensitive modes of chlorophyll, as well as from oxidation-induced structural changes in amino acid residues and the peptide backbone. Oxidation-induced structural changes may play a role in the facilitation and control of electron-transfer reactions involving the primary donor. In this paper, we report that photooxidation of P_{700} in cyanobacterial PSI perturbs a cysteine residue. At 264 and 80 K, a downshift of a SH stretching vibration from 2560 to 2551 cm^{-1} is observed. Such a downshift is consistent with an increase in hydrogen bonding, with a change in C−S−H conformation, or with an electric field effect. Deuterium exchange experiments were also performed. While the perturbed cysteine is in a protein region that is resistant to exchange, other ^{2}H-sensitive vibrational chl and amino acid bands were observed. From the ^{2}H exchange experiments, we conclude that photooxidation of P_{700} perturbs internal or bound water molecules in PSI and that the P_{700}^+-minus-P_{700} spectrum is ^{2}H exchange-sensitive. The results are consistent with structural complexity in the PSI primary donor, as previously suggested [Kim, S., and Barry, B. A. (2000) *J. Am. Chem. Soc. 122,* 4980−4981]. Possible explanations, including a partial enolization of P_{700}^+, are discussed.

Photosystem I (PSI)[1] catalyzes photoinduced electron transfer from reduced plastocyanin to ferredoxin (*1*). This enzyme is found in all organisms that conduct oxygenic photosynthesis. The primary photochemical event in PSI results in the generation of the cation radical, P_{700}^+. Electron transfer proceeds to an acceptor chl molecule, A_0, a phylloquinone, A_1, and iron−sulfur clusters, F_x and F_A/F_B (*2*). The *psaA* and *psaB* subunits form a heterodimer core of PSI and provide the binding sites for P_{700}, A_0, A_1, and F_x (*3*). X-ray diffraction analysis at 2.5 Å resolution (*4*) shows that PSI contains a chl *a*/*a*′ heterodimer, which plays the role of the primary electron donor, P_{700}.

Vibrational spectroscopy can provide detailed structural information about the primary chl donor of PSI (*5*−*11*). Relevant questions concern the structure and environment of P_{700} in both the neutral and cationic states. This information can be obtained by reaction-induced FT-IR spectroscopy. Using light-minus-dark difference techniques, a spectrum associated with the oxidation of P_{700} can be acquired. This spectrum will exhibit contributions from chl vibrational modes that are perturbed by the oxidation reaction. A detailed assignment for this spectrum will furnish structural information concerning the primary donor. In addition, this spectrum will reflect contributions from amino acid residues and adjacent pigments, which are affected by P_{700} oxidation. Such linked structural changes contribute to the free energy of P_{700} oxidation and may play important roles in the control of electron-transfer reactions.

We have acquired a P_{700}^+-minus-P_{700} FT-IR spectrum in PSI, isolated from the cyanobacterium *Synechocystis sp.* PCC 6803. Spectra were obtained for both control and ^{2}H-exchanged samples. These difference spectra exhibit a vibrational band consistent with the perturbation of a cysteine residue upon P_{700} oxidation. ^{2}H exchange experiments indicate that the cysteine is in a region of the protein resistant to exchange. We also conclude that the ester and, possibly, the keto groups of P_{700} and P_{700}^+ are accessible to exchange. Our data suggest that the photooxidation reaction perturbs internal or bound water molecules. These data also provide additional support for previous observations (*9*), which were consistent with dynamic or static complexity in the structure of P_{700}^+.

MATERIALS AND METHODS

Protein Purification. PSI samples were purified from *Synechocystis sp.* PCC 6803 cyanobacterial cultures (*12*). Cyanobacteria were grown under constant illumination in BG-11 media (*13*, *14*). Cells were broken, and membranes were isolated by techniques previously described (*12*). After

† This work was supported by NSF Grant 98-08934 (B.A.B.).

* Address correspondence to this author at the University of Minnesota, 1479 Gortner Ave., St. Paul, MN 55108. Phone: 612-624-6732; Fax: 612-625-5780; Email: barry@biosci.cbs.umn.edu.

‡ Both authors contributed equally to this work.

§ Present address: Department of Biochemistry, 124 Engel Hall, Virginia Polytechnic Institute and State University, Blacksburg, VA 24061.

[1] Abbreviations: bchl, bacteriochlorophyll; chl, chlorophyll; DCPIP, 2,6-dichlorophenolindophenol; EPR, electron paramagnetic resonance spectroscopy; FT-IR, Fourier transform infrared spectroscopy; methyl viologen, 1,1′-dimethyl-4,4′-bipyridinium dichloride; P_{700}, primary electron donor of photosystem I; PSI, photosystem I.

10.1021/bi0110241 CCC: $20.00
Published on Web 11/21/2001

solubilization in dodecyl maltoside and centrifugation, ion exchange chromatography was performed, and PSI-containing fractions, eluting at ionic strengths greater than 53 mM $MgCl_2$, were pooled (*12*). These fractions correspond to the largest chlorophyll-containing peak in the chromatogram. Size exclusion chromatography (data not shown) shows that these fractions are enriched for trimeric PSI complexes, which are the main oligomeric form in cyanobacterial membranes [see (*15*, *16*) and references cited therein]. Before data collection, samples were dialyzed against a buffer containing 5 mM HEPES−NaOH, pH 7.5, and concentrated to 4−5 mg of chl/mL using Centricon 100 filters (Amicon, Beverly, MA). Chlorophyll quantitation was conducted in 100% methanol (*17*, *18*). To control for small preparation-dependent differences in the yield of P_{700}^+, PSI samples were pooled and then compared.

^2H_2O Exchange. Purified PSI was exchanged into a ^2H_2O buffer containing 5 mM HEPES−NaO^2H, p^{2}H 7.5, and 0.05% dodecyl maltoside (Anatrace, Maumee, OH). NaO^2H was purchased from Cambridge Isotope Laboratories, Inc. (Andover, MA), and was 99.9% labeled with ^{2}H. The p^{2}H is reported as the uncorrected meter reading from the pH electrode. The exchange was performed by a series of four dilution (2−20-fold) and concentration steps and the use of a Centricon 100 concentrating device. The concentration of the PSI samples before the first exchange step was in the range from 0.22 to 2.2 mg of chl/mL. To increase the amount of exchange, samples were also incubated for 3 h in ^2H_2O buffer at 6 °C and then frozen and thawed in that buffer. The H_2O PSI control in 5 mM HEPES−NaOH, pH 7.5, and 0.05% dodecyl maltoside was treated identically and simultaneously.

PSI Activity. Oxygen consumption assays (*19*), using the Mehler reaction, were performed on control and ^2H_2O-exchanged cyanobacterial PSI at 25 °C with a YSI 5300 oxygen electrode (Yellow Spring, OH) (*14*). PSI samples consisted of 20 μg of chl, and the buffer contained 0.1 mM DCPIP, 5.0 mM ascorbate, 0.1 mM methyl viologen, 5 mM HEPES−NaOH, pH 7.5, and 0.05% dodecyl maltoside. The ascorbate was made up in a 1 M stock, and NaOH was used to adjust the pH to pH 7.5. The apparent rate of oxygen consumption in the absence of PSI was 16 ± 5 μM O_2 (mg of chl)$^{-1}$ h^{-1}, and this value was subtracted from the PSI rate. PSI oxygen consumption rates under illumination were calculated to be 150 ± 10 μM O_2 (mg of chl)$^{-1}$ h^{-1}. The addition of ferricyanide and ferrocyanide at the concentrations employed for FT-IR spectroscopy had no significant effect on the rate of light-stimulated oxygen consumption. After FT-IR spectroscopy, dehydrated samples were rehydrated with 20 μL of H_2O or ^2H_2O and stored at −70 °C. The light-stimulated oxygen consumption rates in these rehydrated samples were 180−220 μM O_2 (mg of chl)$^{-1}$ h^{-1}.

EPR Spectroscopy. To observe EPR signals from P_{700}^+ under experimental conditions identical to those used for FT-IR spectroscopy, partially dehydrated, cyanobacterial PSI samples, containing 3 mM potassium ferricyanide, 3 mM potassium ferrocyanide, and 100 μg of chl, were employed. Illumination was performed in the cavity with red- and heat-filtered light from a Dolan-Jenner (Woburn, MA) illuminator. The illumination time was 4 min. Data were acquired at 264 and 80 K on a Bruker (Billerica, MA) EMX 6/1 X-band spectrometer, equipped with a Wilmad (Buena, NJ) variable-temperature dewar. At 264 K, spectra were obtained either under illumination or after a 90 min dark-adaptation. At 80 K, spectra were acquired in the dark before illumination and under illumination. Spectral conditions were the following: microwave frequency, 9.2 GHz; microwave power, 0.2 mW; modulation frequency, 100 kHz; modulation amplitude, 3 G; time constant, 1.3 s; sweep time, 42 s.

FT-IR Spectroscopy. Cyanobacterial PSI samples were partially dehydrated and contained 3 mM ferricyanide and 3 mM ferrocyanide (Figures 2 and 3) (*9*) or 11 mM ferricyanide and 11 mM ferrocyanide (Figures 4−9). The ferri/ferrocyanide mixture was added immediately before partial dehydration. For the H_2O and ^2H_2O experiments, the ferri/ferrocyanide mixture was added in H_2O and ^2H_2O, respectively. FT-IR absorption spectra were acquired by ratioing data obtained before illumination to a background. Difference, light-minus-dark, FT-IR data associated with P_{700}^+-minus-P_{700} at 264 K were recorded on a Nicolet (Madison, WI) Magna 550 II spectrometer with a liquid nitrogen cooled MCT-A (mercury cadium telluride) detector using continuous illumination (*20*). CaF_2 and Ge windows were employed. The low-energy detector cutoff was 500 cm^{-1}. Spectral conditions were as follows: resolution, 4 cm^{-1}; mirror velocity, 2.5 cm/s; apodization function, Happ−Genzel; levels of zero filling, 1 (Figures 2 and 3) or 2 (Figures 4−9); data acquisition time, 4.0 min. While one level of zero filling was sufficient to adequately represent the data, two levels of zero filling supplied a smoother interpolation between data points. Data points were acquired at every other zero crossing of the helium−neon laser. Overall, the data acquisition parameters gave a spectral range with a ω_{max} equal to 8000 cm^{-1}. Data were acquired under nonsaturating conditions, in which the energy detected under the cutoff (from 500 to 400 cm^{-1}) was less than 0.5% of the maximum energy. These are conditions in which infrared spectra are known to be photometrically accurate, and there are no saturation effects.

Infrared data associated with P_{700}^+-minus-P_{700} at 80 K were acquired using continuous illumination and a Nicolet 60SXR spectrometer with a liquid nitrogen cooled MCT-B (mercury cadmim telluride) detector and a Hansen liquid nitrogen cryostat (Santa Barbara, CA) (*21*, *22*). CaF_2 and Ge windows were employed. The low-energy detector cutoff was 400 cm^{-1}. Spectral conditions were as follows: resolution, 4 cm^{-1}; mirror velocity, 1.6 cm/s; apodization function, Happ−Genzel; levels of zero filling, 3; data acquisition time, 7.5 min; and temperature, 80 K. Data points were acquired at every other zero crossing of the helium−neon laser; this procedure is consistent with a spectral range with a ω_{max} equal to 8000 cm^{-1}.

At 264 K, spectra were obtained either under illumination, immediately following illumination, or after a 90 min dark-adaptation. At 80 K, spectra were acquired in the dark before illumination and under illumination. The illumination time was 4 min. For both temperatures, the sample absorbance at 1655 cm^{-1} (amide I band) was less than 0.9, and the continuous illumination source was red- and heat-filtered. Data recorded under illumination were ratioed directly to data recorded in the dark. Difference spectra were corrected for small differences in sample concentration and path length. This was accomplished by normalization to either the amide II amplitude (Figures 2 and 3) or the amide I amplitude

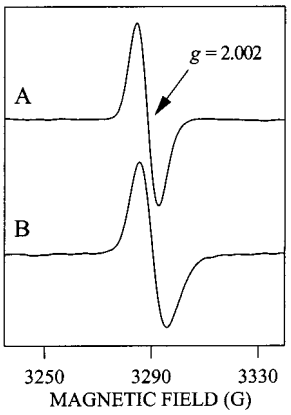

FIGURE 1: Light-minus-dark difference EPR spectra of cyanobacterial PSI at pH 7.5. The P_{700}^+-minus-P_{700} EPR data were obtained at 264 K (A) and at 80 K (B). Samples contained 3 mM potassium ferricyanide and 3 mM potassium ferrocyanide. Spectral conditions are given under Materials and Methods.

(Figures 5−9) in the infrared absorption spectrum. In Figures 2 and 3, the data are the average of 20 (A) or 4 (B) spectra. In Figures 5−9, the data in (A) and (B) are an average of 80 spectra. Data fitting and analysis was performed either with OMNIC (Nicolet, Madison, WI) or with IGOR PRO (Lake Oswego, OR) software.

RESULTS

EPR Control Experiments. The oxidized form of P_{700} can be detected by EPR spectroscopy. P_{700}^+ gives rise to a narrow EPR signal with a *g* value of 2.002 (Figure 1). The EPR data in Figure 1 demonstrate that P_{700}^+ was generated reversibly at 264 K in the presence of 3 mM potassium ferricyanide and 3 mM potassium ferrocyanide. The yield of P_{700}^+ at 264 K (Figure 1A) was 0.18 ± 0.03 spin per 100 chl (*18*). At 80 K, P_{700}^+ was generated by a single illumination of a sample containing 3 mM potassium ferricyanide and 3 mM potassium ferrocyanide. The yield of P_{700}^+ at 80 K was 0.17 ± 0.07 spin per 100 chl and was indistinguishable from the yield at 264 K (Figure 1B). Potassium ferricyanide is expected to act as the electron acceptor at 264 K (*9*) and may be acting as an electron acceptor at 80 K (*8*).

Temperature Dependence of Difference FT-IR Spectra. In Figure 2A, solid line, we present the 2800−1200 cm^{-1} region of the difference FT-IR spectrum obtained by illumination at 264 K. The data in Figure 2A, solid line, are light-minus-dark difference spectra recorded under 4 min of illumination. As expected, vibrational bands in the light-minus-dark difference spectra were significant, relative to the light-minus-light (data not shown) and the dark-minus-dark controls (Figure 2, dotted lines). The 1800−1200 cm^{-1} region of the light-minus-dark spectrum is similar to spectra previously assigned to P_{700}^+-minus-P_{700} (*5*, *8*). This region of the spectrum is dominated by contributions from oxidation-induced changes in the chl macrocycle (*7*). Notice that the 1800−1200 cm^{-1} spectral region was only slightly altered in frequency and not significantly altered in overall amplitude when data were acquired at 80 K (Figure 2B, solid line). Ferricyanide is expected to be reduced upon illumination of PSI. While ferricyanide and ferrocyanide have no fundamental vibrations in the 1800−1200 cm^{-1} region, the C≡N

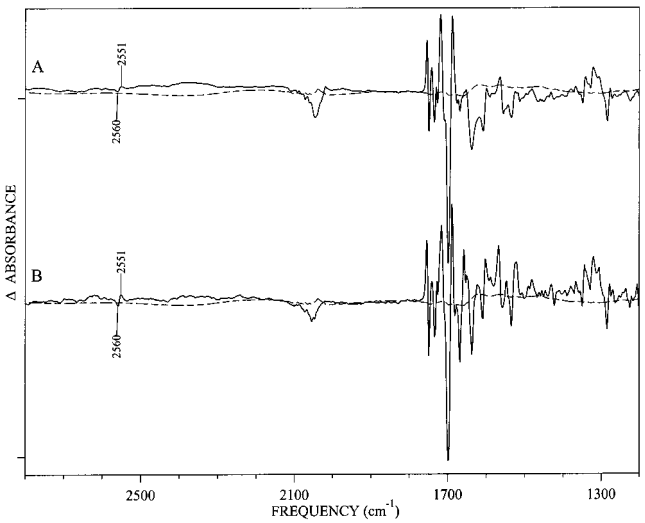

FIGURE 2: The 2800−1200 cm^{-1} region of light-minus-dark difference FT-IR spectra acquired from cyanobacterial PSI at pH 7.5. The P_{700}^+-minus-P_{700} spectrum was obtained at 264 K (A) and at 80 K (B). The dotted lines show the dark-minus-dark spectra at each temperature. Tick marks on the *y*-axis represent $\Delta 4 \times 10^{-3}$ absorbance unit. For clarity, the spectra have been offset from zero. Spectral conditions are given under Materials and Methods.

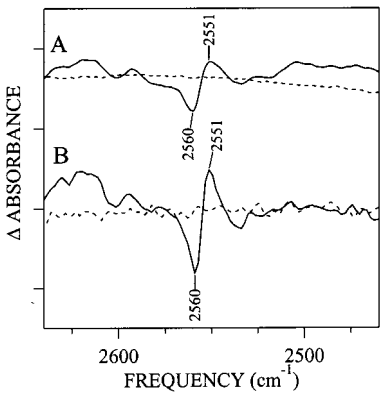

FIGURE 3: The 2640−2460 cm^{-1} region of difference FT-IR spectra acquired from cyanobacterial PSI at pH 7.5. The P_{700}^+-minus-P_{700} spectrum was obtained at 264 K (A) and 80 K (B). These data are repeated from Figure 2 on an expanded scale. The dotted lines show the dark-minus-dark spectra at each temperature. Tick marks on the *y*-axis represent $\Delta 1 \times 10^{-4}$ absorbance unit. The spectra have been offset from zero. Spectral conditions are given under Materials and Methods.

stretching vibration of these compounds is observed between 2200 and 2000 cm^{-1} (*20*).

In Figure 3, the 2640−2460 cm^{-1} region of Figure 2 is presented. Data were obtained at 264 K (Figure 3A, solid line) and at 80 K (Figure 3B, solid line). A derivative-shaped feature, with frequencies of 2560 (neg.) and 2551 (pos.) cm^{-1}, was observed in both data sets. This feature was small, but was clearly significant relative to the noise in the measurement. This was apparent in a comparison of the data (Figure 3, solid lines) to the dark-minus-dark controls obtained on the same sample (Figure 3, dotted lines). The 2560/2551 cm^{-1} spectral feature was also observed in the absence of the ferricyanide/ferrocyanide couple (data not shown). In the 2560−2550 cm^{-1} region, the only fundamental protein vibrational bands come from the SH stretching modes of cysteine residues [see (*23*−*27*) and references cited therein]. Therefore, the derivative-shaped spectral feature at

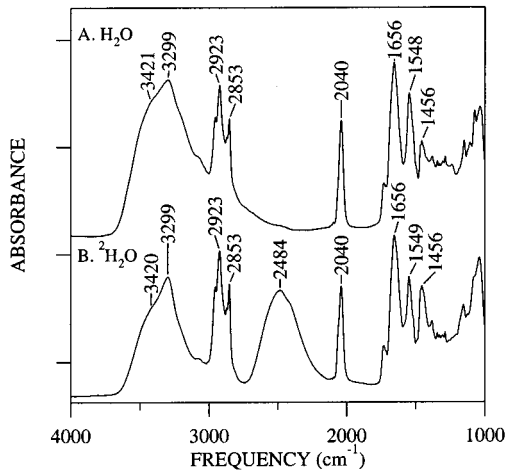

FIGURE 4: Infrared absorption spectra of cyanobacterial PSI in H_2O buffer (A) and ^2H_2O buffer (B) in the spectral region between 4000 and 1000 cm^{-1}. The tick marks on the *y*-axis represent 0.4 absorbance unit. Spectral conditions are given under Materials and Methods.

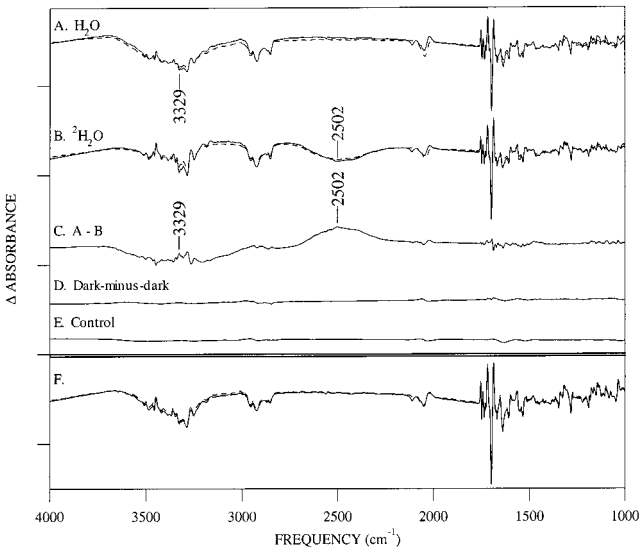

FIGURE 5: Effects of ^2H_2O exchange on the 4000−1000 cm^{-1} region of the light-minus-dark difference FT-IR spectra acquired from cyanobacterial PSI. The P_{700}^+-minus-P_{700} spectrum was obtained under illumination in H_2O buffer (A, solid line) or in ^2H_2O buffer (B, solid line). The isotope-edited, double difference spectrum, H_2O (A, solid line)-minus-^2H_2O (B, solid line), is shown in (C). An averaged dark-minus-dark spectrum is shown in (D). A control double difference spectrum, constructed from data averaged to give (A), is shown in (E). The P_{700}^+-minus-P_{700} spectra, obtained immediately after illumination in H_2O buffer (A, dashed line) or in ^2H_2O buffer (B, dashed line), are also shown. The PSI samples used in (A) and (B) were half of the same pooled PSI preparation. (F) shows a comparison of data acquired through the use of a screen that blocks 70% of the infrared intensity (dashed line) with data acquired without the screen (solid line). These two data sets were also acquired on the same PSI preparation. Tick marks on the *y*-axis represent $\Delta 2 \times 10^{-3}$ absorbance unit. Spectral conditions are given under Materials and Methods.

2560/2551 cm^{-1} is assignable to the S−H stretch of a protonated cysteine residue. Because this cysteine is contributing to the light-minus-dark difference spectrum, P_{700}^+-minus-P_{700}, this cysteine must be perturbed when P_{700} is photooxidized. While the apparent downshift is 9 cm^{-1}, it should be noted that changes in spectral line width and amplitude can influence frequencies in a difference spectrum [see (*22*) and references cited therein].

Effect of ^2H_2O Exchange on the Ground-State FT-IR Spectrum. In Figure 4, the 4000−1000 cm^{-1} region of the FT-IR spectra in H_2O (Figure 4A) and ^2H_2O (Figure 4B) is presented. Spectral contributions from H_2O (3299 cm^{-1}, Figure 4A), ^2H_2O (2484 cm^{-1}, Figure 4B), the C≡N vibration of the ferricyanide/ferrocyanide redox couple (2040 cm^{-1}), and protein backbone vibrations (1656 and 1548 cm^{-1}) are observed. The amide I band (1656 cm^{-1}) is predominantly a CO stretching vibration, and the amide II band (1548 cm^{-1}) arises from a C−N/N−H vibrational mode of the peptide backbone (*28*). While the amide I band is expected to exhibit only modest changes upon deuterium exchange, the amide II band is expected to downshift 90−100 cm^{-1} in ^2H_2O (*28*). The downshifted band will be referred to as amide II′ and is observed in Figure 4B at 1456 cm^{-1}. Therefore, comparison of the amplitudes or integrated areas of the amide II and amide II′ spectral bands gives an estimate of the percent exchange (*29*). Estimates of the amount of exchange were derived from the equation: $f = w'/w$, where w' is the ratio of amide II′ to amide I′ (^2H_2O) and w is the ratio of amide II to amide I (H_2O) (*29*). This calculation gave a value of 20 ± 1% exchange. Larger values, closer to 30% exchange, were calculated using other methods (*29*).

Effect of ^2H_2O Exchange on the Difference FT-IR Spectrum. In Figure 5, we present the effect of ^2H exchange on the 4000−1000 cm^{-1} difference spectrum associated with the oxidation of P_{700}. In Figure 5A, solid line, the spectrum associated with P_{700}^+-minus-P_{700} in H_2O is presented; in Figure 5B, solid line, the spectrum associated with P_{700}^+-minus-P_{700} in ^2H_2O is presented. To give excellent reproducibility, the H_2O and ^2H_2O samples were two halves of the same pooled PSI sample. This eliminates any difference between the spectra due to preparation-to-preparation variation. These spectra are corrected for path length and concentration and so can be directly subtracted, on a one-to-one basis, to give the isotope-edited spectrum, H_2O-minus-^2H_2O, shown in Figure 5C. This isotope-edited spectrum exhibits well-defined vibrational bands. The dark-minus-dark (Figure 5D) and control double difference spectrum (Figure 5E) are shown for comparison. The control double difference spectrum was constructed by one-to-one subtraction of half of the data set acquired in H_2O from the other half of the data. The origin of intense negative and small positive bands in the 2900 cm^{-1} (CH stretching region) region of Figure 5A,B, solid lines, is not known, but similar bands have been reported recently for *Chlamydomonas* PSI (*10*). Small spectral features at approximately 2900 and 2100 cm^{-1} were observed in the double difference spectrum (Figure 5C). Because bands with similar amplitude were observed in the dark-minus-dark controls and control double difference spectra, these bands will not be considered in more detail.

On this scale, it is clear that substitution of ^2H_2O for H_2O resulted in the downshift of a broad spectral feature at 3329 cm^{-1} to 2502 cm^{-1} (Figure 5C). These bands were not observed in the control double difference spectrum (Figure 5E) or in the dark-minus-dark spectrum (Figure 5D). The difference spectra shown in Figure 5A,B, solid lines, were constructed with data obtained in the dark and *under* illumination. An indistinguishable P_{700}^+-minus-P_{700} spectrum was constructed with data obtained in the dark and *after* illumination (Figure 5A,B, dashed lines). This experiment

shows that the broad features are not an artifact of visible illumination. Our data are acquired under conditions in which the infrared detector is not saturated (see Materials and Methods). Confirming the expected photometric accuracy, identical difference spectra were acquired with and without a screen that blocks 70% of the infrared radiation (Figure 5F, solid and dashed lines).

In Figure 5C, the frequency of the 3329 and 2502 cm^{-1} bands suggests a water assignment. However, these features are slightly shifted in frequency from the frequency observed for bulk H_2O and for ^2H_2O in Figure 4. Therefore, the double difference spectrum is consistent with a perturbation of internal or bound water molecules upon photooxidation of the PSI primary donor. While a NH stretching assignment cannot be definitively excluded, we favor the OH stretching assignment because of the intensity and breadth of these spectral contributions. The negative bands are much more intense than any positive vibrational contributions in the OH or O^{2}H stretching region. Such a spectral signature may be consistent with the light-induced movement of internal or bound water molecules from the PSI reaction center to join the solvent.

In addition to the broad water contribution, Figure 5C exhibits narrow ^2H sensitive bands in three other regions which will be discussed in detail below: (A) the 2000−1000 cm^{-1} region; (B) the 3700−3100 cm^{-1} region; and (C) the 2640−2460 cm^{-1} region. These are regions where the control (Figure 5E) and dark-minus-dark spectra (Figure 5D) show no significant contributions (also see Figures 6, 8, 9). Therefore, while the spectral features in the H_2O-minus-^2H_2O double difference spectrum (Figure 5C) are small, these features are clearly significant relative to the noise. The small amplitude of the double difference is expected, because ^2H exchange occurred in ∼20% of the sample.

(A) The 2000−1000 cm^{-1} Region. Contributions from chl oxidation are expected to dominate this spectral region (Figure 6). In addition, amino acid side chain and peptide bond contributions may be observed. In Figure 6A,B, the spectral changes obtained in H_2O and ^2H_2O are shown. The double difference spectrum, H_2O-minus-^2H_2O (Figure 6C), is clearly significant, as assessed by comparison to the dark-minus-dark spectrum (Figure 6D) and to the control double difference spectrum (Figure 6E). Substitution of ^2H_2O for H_2O can alter the spectrum of chl oxidation by substitution of deuterium in hydrogen bonds (*30*). Also, if chl *a* enolizes, the proton at the 13^2 position is exchangeable, and ^2H-induced alterations in frequency and amplitude are expected (*30*).

Chl *a* oxidation upshifts the ester and keto stretching bands of chl *a* in vitro (*7*). Perturbations of macrocycle vibrations are also expected, but are less well characterized compared to carbonyl band effects. Previously, ^2H labeling of the 13^4 methyl group has been used to assign bands to the chl ester group in P_{700}^+-minus-P_{700} (*9*). This ^2H labeling method does not result in isotope incorporation into aspartic or glutamic acid, and, therefore, this method permits spectral contributions from chl and these amino acids to be distinguished in the 1750 cm^{-1} region (*9*, *31*). Four ester C═O bands were assigned to P_{700}^+/P_{700} using that isotope-editing approach (*9*).

Of those four previously assigned ester carbonyl bands, at (pos.) 1754/(neg.) 1749, (pos.) 1742/(neg.) 1735, (pos.) 1730/(neg.) 1726, and (pos.) 1720/(neg.) 1714 cm^{-1}, three

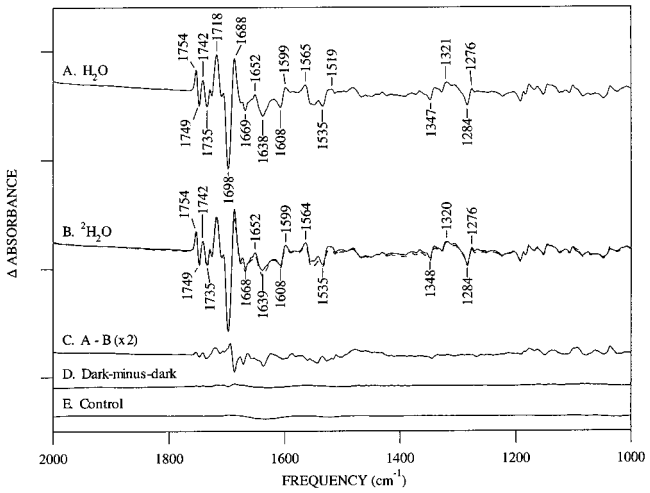

FIGURE 6: Effects of ^2H_2O exchange on the 2000−1000 cm^{-1} region of the light-minus-dark difference FT-IR spectra acquired from cyanobacterial PSI. The P_{700}^+-minus-P_{700} spectrum was obtained in H_2O buffer (A) or in ^2H_2O buffer (B, solid line). (A) is repeated in (B, dashed line) to facilitate comparison. The isotope-edited, double difference spectrum, H_2O (A)-minus-^2H_2O (B), is shown in (C) and is multiplied by a factor of 2 compared to (A) and (B). An averaged dark-minus-dark spectrum is shown in (D). A control double difference spectrum, constructed from data averaged to give (A), is shown in (E). Tick marks on the *y*-axis represent $\Delta 2 \times 10^{-3}$ absorbance unit. Spectral conditions are given under Materials and Methods.

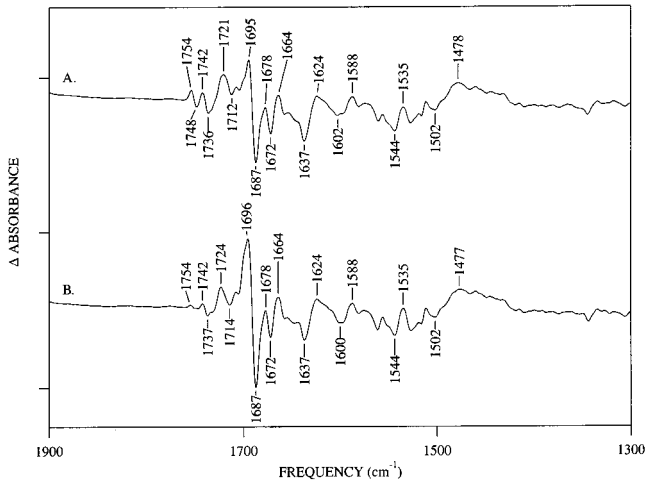

FIGURE 7: Expansion of the isotope-edited spectrum in Figure 6C. The H_2O-minus-^2H_2O spectrum was acquired by a direct one-to-one subtraction in (A). In (B), the H_2O-minus-^2H_2O spectrum was generated by an interactive subtraction designed to minimize spectral contributions in the 1760−1720 cm^{-1} region. The subtraction parameter was 1.06 instead of 1.0. Tick marks on the *y*-axis represent $\Delta 2 \times 10^{-4}$ absorbance unit.

are sensitive to deuterium exchange, because they are observed here in the isotope-edited spectrum (Figure 6C and Figure 7A). These bands, at 1754/1748, 1742/1736, and 1721/1712 cm^{-1}, are present in the H_2O-minus-^2H_2O double difference spectrum, generated either by direct one-to-one subtraction (Figures 6C and 7A) or by a more subjective procedure that is aimed at minimizing spectral contributions in the ester carbonyl region (Figure 7B). While the amplitude of the 1754/1748 cm^{-1} band is small, especially in the spectrum generated by interaction subtraction, the 1742/1736 and 1721/1712 cm^{-1} bands are clearly significant. The 1730/1726 cm^{-1} ester carbonyl band (*9*) does not make a

significant contribution to either double difference spectrum (Figure 7A,B) and thus does not appear to be sensitive to ^{2}H substitution at this level of exchange.

The spectral effects observed are consistent with a ^2H_2O-induced downshift of the frequencies of these bands, caused by ^{2}H exchange into P_{700}^+/P_{700} hydrogen bonds or with ^{2}H exchange into the protonated enol form of P_{700}^+/P_{700}. At this level of exchange, the magnitude of the ^{2}H-induced downshifts appears to be small ($\sim$2 cm^{-1}) and cannot be precisely estimated from the data. Alternatively, ^{2}H exchange may alter the amplitudes of these bands. This can occur, if P_{700}^+ only partially enolizes and if ^{2}H exchange alters the extent of the enolization reaction through an isotope effect. Thus, these results are consistent with the conclusion that P_{700}^+ is hydrogen-bonded (but see Discussion) and/or that P_{700} partially enolizes upon oxidation.

The intense derivative-shaped feature at (pos.) 1718 and (neg.) 1698 cm^{-1} in the P_{700}^+-minus-P_{700} spectrum (Figure 6A) has been assigned to the 13^1 keto vibration, based on comparison to model compounds [(*7*) but see also (*10*)]. We conclude that there is no significant effect of ^{2}H exchange on this band at this level of deuterium exchange, because there are no spectral features in the isotope-edited spectrum with those frequencies (Figure 7). Because four ester bands were identified by isotope labeling, it is reasonable to expect that multiple keto vibrations will also contribute to the spectrum. Partial enolization is expected to lower the force constant of the 13^{1}CO ("keto") stretching vibration, because the introduction of a double bond into the isocyclic ring decreases the force constant for the 13^{1}CO bond (*32*). Therefore, specific isotope labeling of chl is required to identify those lines definitively.

However, suggestive evidence for the 13^{1}CO assignments comes from the deuterium exchange experiment (Figure 6C and Figure 7), where clear frequency shifts are observed in bands between 1700 and 1600 cm^{-1}. A positive band at 1695 cm^{-1} in the H_2O-minus-^2H_2O spectrum may be a 13^{1}CO vibration of P_{700}^+ and may shift to 1687 cm^{-1} ($\Delta = -8$ cm^{-1}) upon deuterium exchange. A positive, negative, positive spectral feature at 1678, 1672, 1664 cm^{-1} appears to arise from a ^{2}H-induced downshift of a derivative-shaped 13^{1}CO band. A negative band at 1637 cm^{-1} may be shifting to 1624 cm^{-1} in ^2H_2O ($\Delta = -13$ cm^{-1}) and may represent an extremely downshifted 13^{1}CO vibrational mode, as suggested previously (*8*). Alternatively, the 1637 cm^{-1} band may arise from a chl macrocycle or amino acid (*10*) vibrational mode that is ^{2}H-sensitive. Other deuterium-sensitive bands are observed in this spectral region. These lines may represent amino acid residues that are exchangeable or hydrogen bonded, or these lines may arise from other chl vibrations that are deuterium-exchange-sensitive. Isotopic labeling experiments are required to address these assignments in a definitive fashion.

(B) The 3700−*3100 cm*$^{-1}$ *Region.* In this region, we may observe the OH and NH stretching vibrations of amino acid residues that are structurally altered when P_{700} is oxidized. A subset of these may be hydrogen bonded to P_{700}. If enolization occurs, then a OH stretching mode of the enol will shift out of this spectral range. In vitro studies suggest that the frequency expected for that OH stretching mode is 3535 cm^{-1} (*30*).

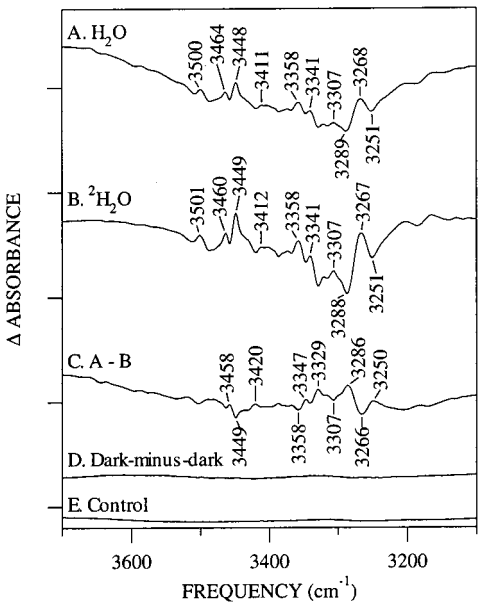

FIGURE 8: Effects of ^2H_2O exchange on the 3700−3100 cm^{-1} region of the light-minus-dark difference FT-IR spectra acquired from cyanobacterial PSI. The P_{700}^+-minus-P_{700} spectrum was obtained in H_2O buffer (A) or in ^2H_2O buffer (B). The isotope-edited, double difference spectrum, H_2O (A)-minus-^2H_2O (B), is shown in (C). A dark-minus-dark spectrum is shown in (D). A control double difference spectrum, constructed from data averaged to give (A), is shown in (E). Tick marks on the *y*-axis represent $\Delta 1 \times 10^{-3}$ absorbance unit. Spectral conditions are given under Materials and Methods.

In Figure 8A,B, the spectral changes obtained in H_2O and ^2H_2O are shown. The double difference spectrum, H_2O-minus-^2H_2O (Figure 8C), is clearly above the noise in the measurements, as assessed by comparison to the dark-minus-dark spectrum (Figure 8D) and to the control double difference spectrum (Figure 8E). Spectral bands are tentatively assigned to OH and NH stretching vibrations of groups that are perturbed by the oxidation reaction. Again, the magnitude of most of the apparent isotope shifts is small.

Our data in the 1800−1200 cm^{-1} region suggest heterogeneity in the structure of P_{700} and P_{700}^+. The 3700−3100 cm^{-1} region is also complex, consistent with those results and with direct or indirect interaction of these amino acid side chains with the primary donor. In addition, it is consistent with chl enolization and other types of interactions, for example, electric field interactions, with amino acid side chains in PSI. Spectral perturbations may also be due to a small equilibrium isotope effect on the structure of PSI (*33*). The assignment of these bands will be explored in the future by isotopic labeling of chl and amino acid residues.

(C) The 2640−*2460 cm*$^{-1}$ *Region.* If the cysteine is in an accessible region of PSI, substitution of ^{2}H for ^{1}H will downshift the stretching vibration at 2560 cm^{-1} by approximately 750 cm^{-1}. Therefore, the effect of ^{2}H exchange on the 2560/2551 cm^{-1} band was investigated. In ^2H_2O buffer, this region of the spectrum is superimposed on the intense O−^{2}H stretching vibration (Figure 5C). This broad spectral contribution was subtracted through the use of a polynomial fitting procedure (Figure 9B,C).

We have not detected any isotope-sensitive lines in the 1900 cm^{-1} region of the ^2H_2O spectrum (data not shown). However, about 50% of the amplitude of the S−H vibrational

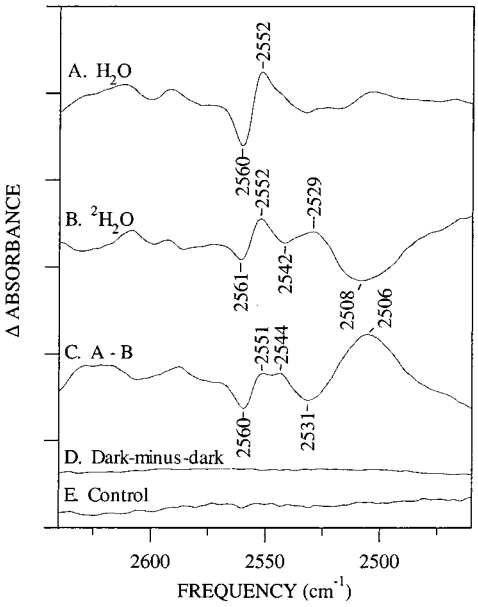

FIGURE 9: Effects of ^2H_2O exchange on the 2640−2460 cm^{-1} region of the light-minus-dark difference FT-IR spectra acquired from cyanobacterial PSI. The P_{700}^+-minus-P_{700} spectrum was obtained in H_2O buffer (A) or in ^2H_2O buffer (B). The isotope-edited, double difference spectrum, H_2O (A)-minus-^2H_2O (B), is shown in (C). To present (B), a background signal from ^2H_2O was fit with a polynomial and subtracted through the use of Igor Pro software. Similar results to (C) were obtained when the subtraction was performed with uncorrected data, and then the double difference spectrum was corrected with the polynomial fit. Tick marks on the *y*-axis represent $\Delta 5 \times 10^{-5}$ absorbance unit. Spectral conditions are given under Materials and Methods. (D) and (E) were generated as described in Figure 8.

band at 2560/2552 cm^{-1} shows an apparent shift to 2544 and 2531 cm^{-1} upon ^2H exchange (Figure 9C). While this is not consistent with direct substitution of ^2H for ^1H in the S−H bond, this shift may be consistent with a small effect of deuterium substitution on the tertiary structure of PSI [reviewed in (*33*, *34*)]. See the discussion for a detailed description of the factors that influence SH frequencies. Alternatively, the 2544/2531 cm^{-1} band could represent a downshifted O^{2}H or N^{2}H vibrational mode. We conclude that the S−H group may be in a region of the protein that is relatively resistant to exchange. The new negative band at 2506 cm^{-1} in the isotope-edited spectrum (Figure 9C) may be the isotope-shifted component of an OH or NH stretching vibration.

Candidates for Spectral Contributors. A spectral feature with identical frequencies (2560/2551 cm^{-1}) was also observed upon oxidation of the primary bacteriochlorophyll donor (P_{798}) in the *Heliobacterium modesticaldum* reaction center (*35*). Growth of that organism on ^2H_2O was shown to downshift the 2560/2551 cm^{-1} spectral feature, supporting the assignment of this band to an X−H stretching vibration (*35*). Moreover, the vibrational band was insensitive to ^2H_2O exchange (*35*).

Taken together, these observations imply similarities in the structural and functional role of cysteine residues in the heliobacterial reaction center and in cyanobacterial photosystem I. A close evolutionary relationship between cyanobacterial photosystem I and the heliobacterial photosystem has been deduced from other types of analysis (*36*−*38*). P_{700} is coordinated by histidine residues in the psaA and psaB subunits, which form the heterodimeric core of PSI (*4*, *39*, *40*). It is hypothesized that P_{798} is ligated by residues in the pshA subunit, which is expected to form the homodimer core of this reaction center (*36*, *37*). Accordingly (Figure 10), we performed a CLUSTAL sequence alignment (*41*) of amino acid sequences derived from the *Synechocystis sp.* PCC 6803 *psaA* gene (*42*, *43*), the *Synechocystis sp.* PCC 6803 *psaB* gene (*42*, *43*), and the *Heliobacillus mobilus pshA* gene (*36*, *37*). BLAST (*44*) sequence alignments gave similar results (data not shown). The *Synechocystis* amino acid sequences have approximately 30% overall similarity to the *H. mobilus pshA* sequence (Figure 10). Two cysteines were conserved in the *psaA*, *psaB*, and *pshA* sequences (Figure 10); these residues provide ligation to iron in the F_x iron−sulfur cluster in PSI and presumably provide F_x ligation in the heliobacterial reaction center (*3*, *4*, *45*). The only other conserved cysteine in any sequence is residue C444 in the *Synechocystis psaA* sequence, which is conserved in 37 known *psaA* sequences [also see (*3*)]. While there is no corresponding conserved cysteine in this position in *pshA* (Figure 10), C317 in the *Helobacillus pshA* sequence may be in a similar tertiary structural environment (see Discussion). Therefore, we suggest that C444 in the psaA subunit may be a candidate for the cysteine that undergoes a structural perturbation upon oxidation of P_{700} in *Synechocystis* 6803. However, other candidates cannot be ruled out, at this point. This cysteine is not predicted to be in close proximity to the primary chl donor (*4*), so if the perturbed cysteine is C444, it must be perturbed by a propagated, light-induced conformational change in the PSI reaction center (see Discussion and Figure 11). Such conformational changes have been detected in the bacterial reaction center (*46*).

DISCUSSION

Several published reports demonstrate that photooxidation of P_{700} in PSI leads to a difference FT-IR spectrum reflecting perturbations of chlorophyll carbonyl and macrocycle vibrations (*9*−*11*, *47*, *48*). For example, oxidation of chl in vitro has been shown to cause an upshift of carbonyl stretching vibrations (*7*, *9*, *47*, *48*). However, structural changes in the protein matrix of PSI, which are coupled to the photooxidation reaction, have not been extensively characterized. Such coupled reactions can play important roles in adjusting the energetics of the electron-transfer reactions and can be identified by difference FT-IR spectroscopy (*49*). Two types of such coupled reactions are expected. The first includes perturbations of groups in close proximity to the primary donor. For example, oxidation may cause bond strength alterations, which, in turn, cause changes in hydrogen bonding interactions with amino acid side chains in the environment. The second includes perturbations occurring at some distance from the primary donor and mediated by indirect interactions. For example, oxidation of the primary donor may generate an electric field, which causes helix dipole rearrangements and, thus, indirectly mediates coupled structural changes at some distance.

^2H Exchange in Cyanobacterial PSI. To investigate the interaction of the primary donor with the environment, we have employed a ^2H exchange experiment. To our knowledge, this is the first report of significant ^2H exchange in PSI [see (*8*) and references cited therein]. Based on the change in relative amplitudes of the amide II and amide II′

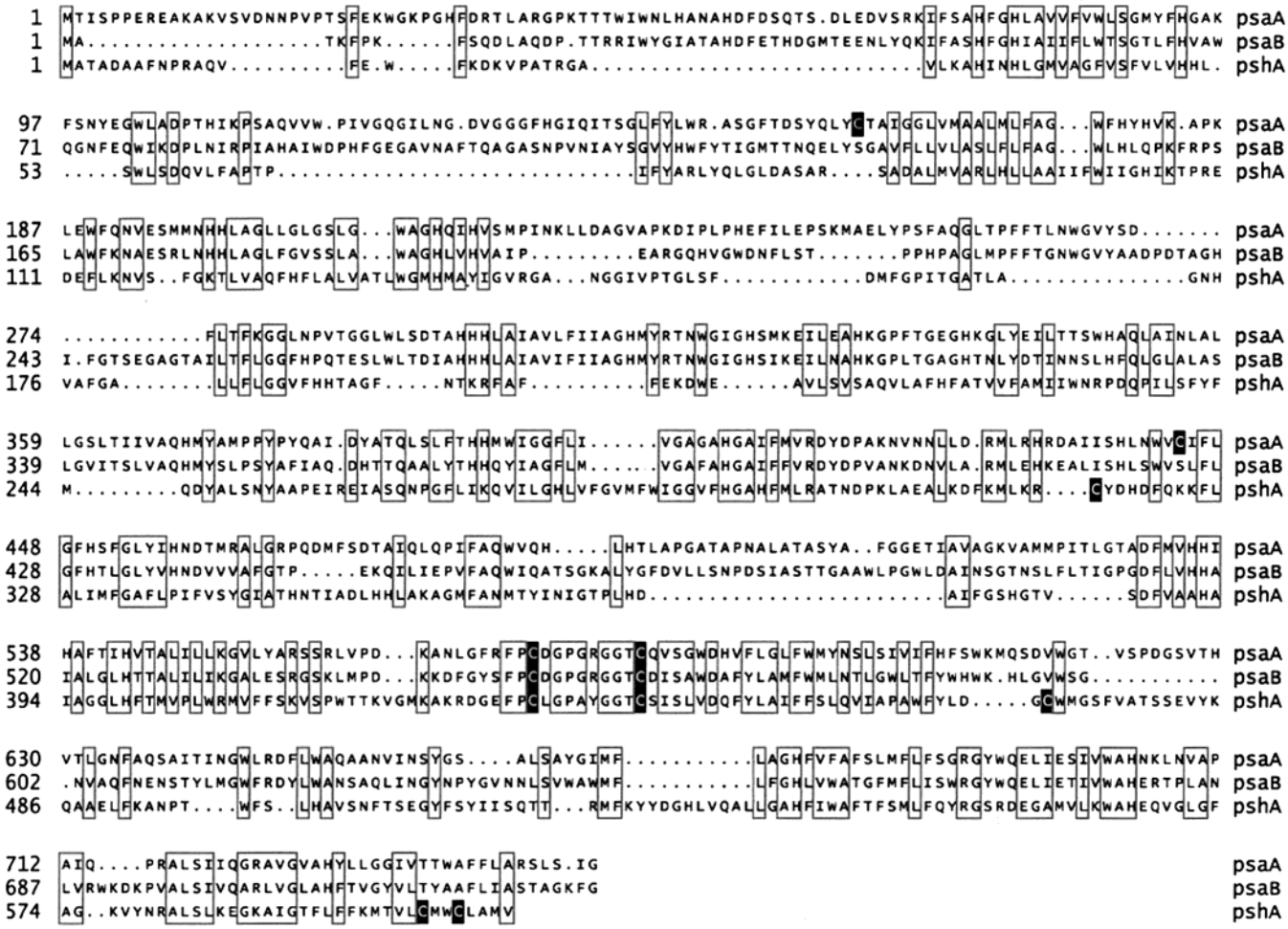

FIGURE 10: Comparison of polypeptide sequences for the *Synechocystis sp.* 6803 psaA subunit, the *Synechocystis sp.* 6803 psaB subunit, and the *Heliobacterium mobilis* pshA subunit. Sequences were derived from the nucleotide sequences, and alignments were generated using CLUSTAL methods (*41*) and a gap penalty of 10. Identity and similarity across all three sequences are highlighted in boxes. Cysteine residues are highlighted in black boxes. A dot represents a gap introduced to maximize identity. Entrez-GenBank accession numbers for *Synechocystis psaA*, *Synechocystis psaB*, and *H. mobilis pshA* are CAA41629 (*42*, *43*), CAA41630 (*42*, *43*), and T31454 (*36*, *37*), respectively.

bands in the FT-IR absorption spectrum, ^{2}H exchange occurred in ~20% of PSI. This is a reasonable value for hydrophobic proteins, which are typically resistant to deuterium exchange in transmembrane regions [for example, see (*50*, *51*), but also see, for example, (*52*)].

^{2}H exchange will alter the vibrational frequencies of several classes of vibrational bands. First, vibrational bands involving hydrogen displacement in titratable groups will be downshifted if there is a substitution of deuterium for hydrogen. Second, vibrational bands arising from hydrogen-bonded functional groups will be altered upon deuterium substitution into the hydrogen bond. The vibrational shifts expected for a X−H stretching mode can be quite substantial, on the order of hundreds of cm^{-1}, while the vibrational shifts expected for hydrogen-bonded species are modest and will depend on hydrogen bond strength and the mode of hydrogen bonding. Third, there may be isotope effects on the three-dimensional structure of the complex (*33*), which could give rise to small changes in vibrational frequency.

Our data show that three of the four previously identified (*9*) ester carbonyl bands in the P_{700}^+-minus-P_{700} spectrum are sensitive to ^{2}H exchange. Also, we have proposed candidates for ^{2}H exchange sensitive 13^1 CO vibrations. These ^{2}H exchange results suggest either that the carbonyl groups of P_{700}^+ are hydrogen-bonded or that P_{700}^+ enolizes, creating an exchangeable proton at position 13^2 (*30*). One explanation for these ^{2}H exchange results is that a significant amount of the unpaired spin density in P_{700}^+ is delocalized on chl *a*′, which is hydrogen bonded (*4*). However, in recent work, 85% of the P_{700}^+ unpaired spin density was reported to be localized on the chl *a* monomer (*53*), and this monomeric chl is not hydrogen-bonded (*4*). It seems unlikely that ~15% of the P_{700}^+ spin could be detected in our experiments.

A second possible explanation may be the spectral interpretation of (*10*), which postulates that the hydrogen-bonded chl *a*′ monomer contributes to the PSI photooxidation spectrum, but that the keto CO frequency for this monomer downshifts, instead of upshifts. However, the spectral assignments suggested in (*10*) do not account for the ^{2}H shifts observed in our *Synechocystis* data, and significant differences were observed between spectra acquired from *Chlamydomonas* and *Synechocystis* PSI (*10*).

An enolization reaction is a third possible explanation of these results. Chl *a* is a β-keto ester and thus can tautomerize to generate the enol form, but the enol is not the favored structure in solution (*32*). It has been suggested previously that P_{700}^+ may enolize, due to a protein interaction that favors the tautomer, and that such an enolization reaction would account for the low midpoint potential of P_{700} (*32*). A partial

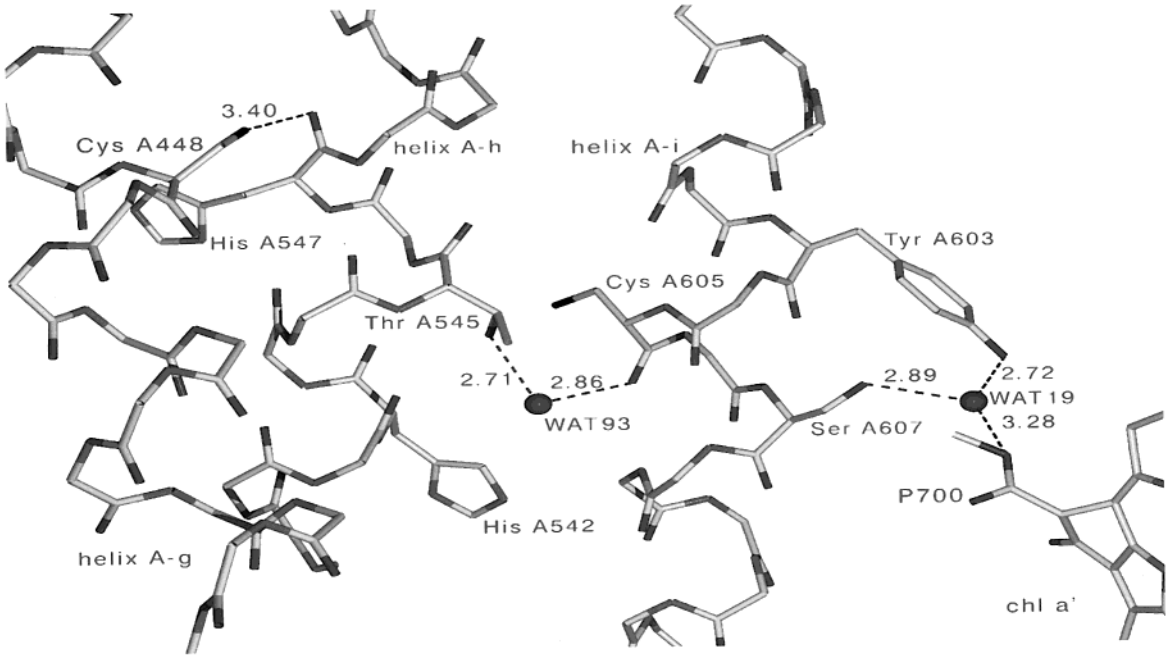

FIGURE 11: View from the X-ray structure of *Synechococcus* PSI showing psaA C448, the chl *a*′ monomer in P_{700}, water molecules 19 and 93, and potential interactions (*4*). The psaA polypeptide is the only PSI subunit shown. The chl hydrophobic tail and some amino acid side chains are not shown for clarity. Only a subset of the possible interactions is illustrated in this view. The PDB file (accession number IJB0) was graciously provided by Dr. P. Fromme. The figure was drawn using Swiss-PdbViewer [v 3.6 beta; www.expasy.ch/spdbv; (*63*)] and rendered using POV-Ray (v 3.1; www.povray.org).

enolization reaction may explain both our ^2H exchange results and our previous observation (*9*) of multiple (>2) ester bands for P_{700}^+. In this regard, the observation of a spectral band at 1637 cm^{-1} that is sensitive to ^2H exchange is noteworthy. If this frequency arises from the 13^1 CO stretching vibration, this vibrational mode is shifted to low energies when compared to $13^1C{=}O$ frequencies observed for chl *a* in solution (*7*, *48*), consistent with the enolization hypothesis. However, other possible explanations and origins of the 1637 cm^{-1} band cannot be excluded at this time (*10*). Interestingly, distorted bond angles are observed in ring V of the non-hydrogen-bonded chl *a* monomer in P_{700} (Dr. Petra Fromme, personal communication). Such distortions may be consistent with a partial enolization reaction.

Recently, the effect of ^2H substitution at nonexchangeable positions has been investigated in cyanobacterial PSI. This experiment was conducted by growth of cyanobacteria on ^2H_2O. This experiment led to a preliminary assignment of bands to P_1 and P_2, which were attributed to the two monomeric halves of the P_{700} dimer (*8*). However, this method of assignment is not definitive, and this ^2H exchange work and our previous labeling results (*9*) have shown that the FT-IR spectrum associated with P_{700} oxidation is much more complex. Note that an alternate set of assignments for the *Chlamydomonas* P_{700} spectrum has been suggested recently (*10*). The applicability of these assignments for cyanobacterial PSI remains to be evaluated.

Another important result acquired from our ^2H exchange is the observation of a negative, broad water band (*54*−*56*) in the P_{700}^+-minus-P_{700} spectrum. This feature has not been reported in some previous PSI studies, because the concentration of solvent water was too high to obtain accurate data in this region (*10*). A similar broad negative band was observed in ref *8*, but was not discussed. The observation of broad intense negative water bands in the P_{700}^+-minus-P_{700} difference spectrum is consistent with displacement of internal water molecules to solvent. The observed frequency of the broad negative band, which is shifted from the bulk, is also consistent with an assignment to internal water molecules. The 2.5 Å crystal structure (*4*) places several water molecules in the vicinity (<7 Å) of P_{700} (Figure 11, see discussion below). The perturbation of water by photooxidation may occur through a long-range structural interaction, and one possible pathway for such an interaction is shown in Figure 11. Other interaction pathways may exist as well.

Identity of the Perturbed Cysteine. In this report, we have observed for the first time a structural change of a cysteine residue, which is coupled to the photooxidation of P_{700} in cyanobacterial PSI. Perturbation of a S−H vibrational band has also been reported upon oxidation of the primary chlorophyll donor, P_{798}, in a reaction center from *Heliobacterium modesticaldum* (*35*). Given the sensitivity of the S−H stretching frequency to its physical state (see discussion below), the fact that a S−H band with identical frequencies is observed in *Synechocystis* PSI and in the heliobacterial reaction center is of significance. These results imply that the immediate environment of the perturbed cysteine is indistinguishable in the two reaction centers. These results also imply that the cysteine may be functionally significant. Therefore, our vibrational analysis provides spectroscopic evidence for a close structural/functional relationship between heliobacterial photosynthesis and PSI, as suggested previously on the basis of other considerations (*36*−*38*).

To identify possible candidates for the perturbed cysteine observed in our infrared data, an alignment of the *psaA*, *psaB*, and *pshA* sequences was performed. The psaA and psaB polypeptides are each highly conserved in all sequences currently available [see also (*3*)]. To date, the *pshA* sequence from the anoxygenic heliobacterium *Heliobacterium modes-*

ticaldum is not known. Accordingly, the *pshA* sequence (*36*, *37*) from *Heliobacillus mobilus* was compared to the *psaA* and *psaB* sequences. The level of identity comparing all three sequences was approximately 20%. The highest level of conservation was observed in the carboxyl-terminal half of the *pshA* sequence (Figure 10). This part of the *psaA* and *psaB* sequence contains the histidine ligands (H676 in psaA, H651 in psaB) for P_{700} (*4*, *39*, *40*), as well as the cysteine ligands (C574 and C583 in psaA, C556 and C565 in psaB) for the F_x iron−sulfur cluster (*4*, *57*). As shown in Figure 10, the *pshA* sequence contains a conserved histidine at position 538, which is a candidate for a ligand to the primary donor. The *pshA* sequence also contains conserved cysteines (C433 and C442), which are putative ligands for the F_x iron−sulfur cluster in this reaction center. These cysteine ligands are in the deprotonated thiolate form and cannot contribute a S−H stretching vibration to the spectrum.

The psaB subunit contains no additional cysteines that are conserved in all *psaB* sequences. The psaA subunit contains a single additional cysteine (C444) that is conserved in all *psaA* examples sequenced, as previously noted (*3*). This cysteine corresponds to C448 in the *Synechococcus psaA* sequence, and this homologous cysteine is found in helix A-g of *Synechococcus* PSI (*4*). There is no conserved cysteine predicted at this position in the pshA polypeptide (Figure 10). However, the *pshA* sequence has a cysteine (C317) that is predicted to be seven residues away in the sequence alignment (Figure 10). If the region containing C317 is α-helical [but see (*45*)], both cysteines may fall on the same face of the helix in the pshA and psaA polypeptides. Because the properties of the cysteine are likely to be dependent on tertiary structural factors, such as helix packing, this cysteine could be in a similar environment in the two reaction centers, even though the immediate primary sequence is not similar. Note that the *pshA* sequence has three additional residues, which are also candidates for the cysteine that contributes to the heliobacterial difference FT-IR spectrum (*35*). Due to the low level of sequence identity between *psaA/psaB* and *pshA*, other possible candidates cannot be excluded at the present time.

We searched the *Synechococcus* PSI X-ray structure (*4*) for cysteines in the psaA and psaB polypeptides and measured the distance between each cysteine and P_{700}^+. In each polypeptide, two cysteines (C578/587 in psaA and C565/574 in psaB) ligate F_x. These cysteines are not candidates for the perturbed cysteine because they are deprotonated. As stated above, the homologue of *Synechocystis* C444 is *Synechococcus* C448. The sulfur atom of C448 is 27 Å from the Mg^{2+} in each monomeric chl in P_{700}. Other cysteines are 46−52 Å (psaA-C160), 20−22 Å (psaA-C605), and 37−40 Å (psaB−C343) from the two monomeric chls of P_{700}; none of these cysteines are conserved in *Synechocystis psaA* or *psaB*. No other PSI polypeptide has a cysteine that is closer than ∼30 Å from the primary donor. From this analysis, it is clear that the effect of P_{700} on the cysteine must be a long-range structural interaction, which is detectable by FT-IR spectroscopy. This is of significance, because it is sometimes assumed that FT-IR spectroscopy is sensitive only to short-range interactions.

As shown in Figure 11, there is a potential pathway for a long-range interaction between P_{700} and psaA C448. C448 has a potential hydrogen-bonding interaction with a peptide carbonyl group provided by psaA H547. A nonconserved cysteine, C605, is found between C448 and P_{700} in this view of the *Synechococccus* PSI structure. This potential pathway involves two water molecules, which link adjacent α-helices through potential hydrogen-bonding interactions (Figure 11). Other possible pathways for a structural interaction may exist, and not all potential interactions are shown in Figure 11.

Mechanisms for Cysteine Perturbation in Cyanobacterial PSI. The nature of the long-range cysteine perturbation can be elucidated from the literature on thiols, cysteine, and cysteine-containing proteins [see (*23*−*27*) and references cited therein]. Based on this literature, there are several possible interpretations to explain an apparent 9 cm^{-1} downshift of a S−H cysteine mode upon generation of the chl cation radical, as well as to explain the 2560 and 2552/1 cm^{-1} frequencies of the observed bands. The first interpretation of the observed, apparent 9 cm^{-1} downshift is a change in S−H hydrogen bonding. In non-hydrogen-bonding solvents in which thiols are not self-associated, the S−H stretching frequency is observed above 2678 cm^{-1} (*26*). Formation of hydrogen bonds in which the S−H group is the hydrogen bond donor results in a downshift and broadening of the S−H stretching vibration (*26*). This is the expected effect of hydrogen bond donor interactions on stretching frequencies (*34*). This effect on υ_{SH} can be substantial, with downshifts of up to 40 cm^{-1} possible in the solution state and larger frequency shifts observed in the crystalline state (*26*). On the other hand, formation of hydrogen bonds in which the sulfur is a hydrogen bond acceptor results in modest upshifts (∼4 cm^{-1}) of υ_{SH} (*26*).

The second interpretation of the observed 9 cm^{-1} downshift is a change in rotamer conformation at the C−S bond in cysteine. Although the S−H vibrational band is a relatively isolated stretching mode, vibrational studies and normal-mode analysis of thiol model compounds suggest that changes in C−S−H rotamer conformation can alter υ_{SH} in cysteine by approximately 10 cm^{-1} (*26*, *58*). Effects on υ_{CS} are also expected (*26*, *58*). However, because the frequency of this vibrational band is expected at less than 1000 cm^{-1}, it is not observable in these FT-IR experiments, which employ calcium fluoride windows.

The third interpretation of the observed 9 cm^{-1} downshift is that production of the chl cation radical generates an electric field, which shifts υ_{SH} of cysteine [for example, see (*59*)]. Electric fields cause shifts in the frequency and the amplitude of vibrational lines; these shifts can be substantial (>100 cm^{-1}) and either to higher or to lower energy (*60*−*62*). For example, when CO is bound to myoglobin, an inverse linear relationship between the calculated electrostatic potential and υCO has been established. Shifts of 60−70 cm^{-1} were observed (*62*). The direction and magnitude of the shift are determined theoretically by two terms involving both the permanent and the electric-field-induced dipole moment: $-E_{||}\delta\mu^0/\delta r$ and $-0.5E_{||}\delta\mu^{induced}/\delta r$, where μ^0 is the permanent dipole moment, $\mu^{induced}$ is the dipole moment induced by the field, r is the stretching normal coordinate, and $E_{||}$ is the component of the electric field component that is parallel to the direction of the vibration (*60*, *61*). For a positive field, the second term will be negative, and the sign of the frequency shift is determined by the sign of the permanent dipole moment derivative (*60*, *61*).

A fourth interpretation of the observed 9 cm^{-1} downshift is that alterations in the polarity/dielectric constant of the medium, caused by photooxidation of the primary donor, result in shifts of υ_{SH} of cysteine. To our knowledge, there has been no study examining this effect for thiol model compounds in the absence of hydrogen-bonding changes, so we will not consider this possibility further.

Based on the above literature, the observed S−H band in the dark state of PSI (neg. 2560 cm^{-1}) arises most likely from a hydrogen-bonded S−H group, in which the cysteine is a hydrogen bond donor (S−H−X). The apparent 9 cm^{-1} downshift (pos. 2551 cm^{-1}), observed when P_{700}^+ is photooxidized, is consistent with a modest increase in hydrogen bonding to the thiol hydrogen, with a change in rotamer conformation at the C−S−H single bond, or with an electric field effect on the S−H stretching mode. Data presented here suggests that the cysteine is in a region of PSI that is relatively resistant to ^2H exchange.

In these reaction-induced experiments, the trigger for the S−H perturbation is the generation of the cation radical, and the perturbative mechanism must be long-range (see discussion above). If the perturbation is due to an electric field effect, the localization of charge in the cation radical, the distance between the radical and the cysteine, and the detailed placement of amino acid residues, bound waters, etc. must be similar. If the long-range cysteine perturbation is due to a hydrogen-bonding change, the cysteine must be involved in an extensive hydrogen-bonded network, which is perturbed by oxidation of the primary donor and ensuing structural changes (see Figure 11 for one example of such a network involving C448).

Alternatively, steric forces, induced by photooxidation of the primary donor, could force a change in C−S−H rotamer conformation in both reaction centers. This explanation presupposes a change in packing of PSI helices or side chains, when P_{700} is photooxidized. Significant changes in the structure and in the position of an acceptor side quinone have been observed in reaction centers from purple nonsulfur bacteria under illumination (*46*). In model compounds, there is a small energy barrier between the predominant rotamer conformation and other rotamers, giving rise to a predicted temperature dependence in spectral amplitudes (*58*). Consistent with this explanation, the observed temperature dependence of the S−H band (Figure 3) provides support that the observed downshift results from a change in C−S−H rotamer conformation. In this scenario, as the temperature is lowered, the preferred rotamer conformation, with a vibrational frequency 2560 cm^{-1}, is predominant, leading to an increased amplitude of the cysteine band in the difference spectrum (compare Figure 3A and 3B, solid lines).

SUMMARY

We report here the results of a ^2H exchange experiment on the P_{700}^+-minus-P_{700} spectrum, which may be consistent with partial enolization of the primary chlorophyll donor. We also report that perturbation of a cysteine is coupled to photooxidation of the primary donor in cyanobacterial photosystem I. Future work will employ specific isotopic labeling of chlorophyll, to probe the proposed enolization of P_{700} and site-directed mutagenesis of cysteine, to identify its possible function and location in the primary sequence.

ACKNOWLEDGMENT

We thank Dr. R. Hutchison for assistance with 80 K FT-IR data acquisition, Drs. E. J. Wojcik and L. Anderson for assistance with sequence alignment, E. C. Raulfs for assistance in figure preparation, and Drs. R. Brooker and P. Fromme for helpful discussions.

REFERENCES

1. Golbeck, J. H. (1994) in *The Molecular Biology of Cyanobacteria* (Bryant, D. A., Ed.) pp 319−360, Kluwer Academic Publishers, Dordrecht, The Netherlands.
2. Brettel, K. (1997) *Biochim. Biophys. Acta 1318*, 322−373.
3. Bryant, D. A. (1992) in *The Photosystems: Structure, Function and Molecular Biology* (Barber, J., Ed.) pp 501−549, Elsevier, Amsterdam.
4. Jordan, P., Fromme, P., Witt, H. T., Klukas, O., Saenger, W., and Krauss, N. (2001) *Nature 411*, 909−917.
5. Tavitian, B. A., Nabedryk, E., Mantele, W., and Breton, J. (1986) *FEBS Lett. 201*, 151−157.
6. Moenne-Loccoz, P., Robert, B., Ikegami, I., and Lutz, M. (1990) *Biochemistry 29*, 4740−4746.
7. Nabedryk, E., Leonhard, M., Mantele, W., and Breton, J. (1990) *Biochemistry 29*, 3242−3247.
8. Breton, J., Nabedryk, E., and Leibl, W. (1999) *Biochemistry 38*, 11585−11592.
9. Kim, S., and Barry, B. A. (2000) *J. Am. Chem. Soc. 122*, 4980−4981.
10. Hastings, G., Ramesh, V. M., Wang, R., Sivakumar, V., and Webber, A. (2001) *Biochemistry* (in press).
11. Hastings, G., and Sivakumar, V. (2001) *Biochemistry 40*, 3681−3689.
12. Noren, G. H., Boerner, R. J., and Barry, B. A. (1991) *Biochemistry 30*, 3943−3950.
13. Rippka, R., Derulles, J., Waterbury, J. B., Herdman, M., and Stanier, R. (1979) *J. Gen. Microbiol. 111*, 1−61.
14. Barry, B. A. (1995) *Methods Enzymol. 258*, 303−319.
15. Kruip, J., Karapetyan, N. V., Terekhova, I. V., and Rögner, M. (1999) *J. Biol. Chem. 274*, 18181−18188.
16. Wenk, S.-O., and Kruip, J. (2000) *J. Chromatogr., B 737*, 131−142.
17. Lichtenthaler, H. K. (1987) *Methods Enzymol. 148*, 350−382.
18. Noren, G. H., and Barry, B. A. (1992) *Biochemistry 31*, 3335−3342.
19. Allen, J. F., and Holmes, N. G. (1986) in *Photosynthesis, energy transduction a practical approach* (Hipkins, M. F., and Baker, N. R., Eds.) pp 51−101, IRL Press, Oxford.
20. Kim, S., and Barry, B. A. (1998) *Biophys. J. 74*, 2588−2600.
21. Steenhuis, J. J., and Barry, B. A. (1996) *J. Am. Chem. Soc. 118*, 11927−11932.
22. Steenhuis, J. J., and Barry, B. A. (1997) *J. Phys. Chem. B 101*, 6652−6660.
23. Madec, C., Lauransan, J., and Garrigou-Lagrange, C. (1980) *Can. J. Spectrosc. 25*, 47−55.
24. Susi, H., Byler, M. D., and Gerasimowicz, W. V. (1983) *J. Mol. Struct. 102*, 63−79.
25. Moh, P. P., Flamingo, F. G., and Alben, J. O. (1987) *Biochemistry 26*, 6243−6249.
26. Li, H., and Thomas, G. J. (1991) *J. Am. Chem. Soc. 113*, 456−462.
27. Rath, P., Bovee-Geurts, P. H. M., DeGrip, W. J., and Rothschild, K. J. (1994) *Biophys. J. 66*, 2085−2091.
28. Krimm, S., and Bandekar, J. (1986) in *Advances in Protein Chemistry* (Anfinsen, C. B., Edsall, J. T., and Richards, F. M., Eds.) pp 181−364, Academic Press, New York.
29. Rath, P., DeGrip, W. J., and Rothschild, K. J. (1998) *Biophys. J. 74*, 192−198.
30. Ballschmiter, K., and Katz, J. J. (1969) *J. Am. Chem. Soc. 91*, 2661−2677.
31. Kim, S., Patzlaff, J., Krick, T., Ayala, I., Sachs, R. K., and Barry, B. A. (2000) *J. Phys. Chem. B 104*, 9720−9727.

32. Wasielewski, M. R., Norris, J. R., Shipman, L. L., Lin, C., and Svec, W. A. (1981) *Proc. Natl. Acad. Sci. U.S.A. 78*, 2957−2961.
33. Schowen, K. B., and Schowen, R. L. (1982) *Methods Enzymol. 87*, 551−606.
34. Pimentel, G. C., and McClellan, A. L. (1960) *The Hydrogen Bond*, W. H. Freeman and Co., San Francisco.
35. Noguchi, T., Fukami, Y., Oh-oka, H., and Inoue, Y. (1997) *Biochemistry 36*, 12329−12336.
36. Liebl, U., Mochensturm-Wilson, M., Trost, J. T., Brune, D. C., Blankenship, R., and Vermaas, W. (1993) *Proc. Natl. Acad. Sci. U.S.A. 90*, 7124−7128.
37. Xiong, J., Inoue, K., and Bauer, C. E. (1998) *Proc. Natl. Acad. Sci. U.S.A. 95*, 14851−14856.
38. Xiong, J., Fischer, W. M., Inoue, K., Nakahara, M., and Bauer, C. E. (2000) *Science 289*, 1724−1730.
39. Krauss, N., Schubert, W. D., Klukas, O., Fromme, P., Witt, H. T., and Saenger, W. (1996) *Nat. Struct. Biol. 3*, 965−973.
40. Redding, K., MacMillan, F., Leibl, W., Brettel, K., Hanley, J., Rutherford, A. W., Breton, J., and Rochaix, J.-D. (1998) *EMBO J. 17*, 50−60.
41. Thompson, J. D., Higgins, D. G., and Gibson, T. J. (1994) *Nucleic Acids Res. 22*, 4673−4680.
42. Smart, L. B., and McIntosh, L. (1991) *Plant. Mol. Biol. 17*, 959−971.
43. Kaneko, T., Sato, S., Kotani, H., Tanaka, A., Asamizu, E., Nakamura, Y., Miyajima, N., Hirosawa, M., Sugiura, M., Sasamoto, S., Kimura, T., Hosouchi, T., Matsuno, A., Muraki, A., Nakazaki, N., Naruo, K., Okumura, S., Shimpo, S., Takeuchi, C., Wada, T., Watanabe, A., Yamada, M., Yasuda, M., and Tabata, S. (1996) *DNA Res. 3*, 109−136.
44. Altschul, S. F., Gish, W., Miller, W., Myers, E. W., and Lipman, D. J. (1990) *J. Mol. Biol. 215*, 403−410.
45. Amesz, J. (1995) in *Anoxygenic photosynthetic bacteria* (Blankenship, R. E., Madigan, M. T., and Bauer, C. E., Eds.) pp 687−697, Kluwer Academic Publishers, Dordrecht.
46. Stowell, M. H. B., McPhillips, T. M., Rees, D. C., Soltis, S. M., Abresch, E., and Feher, G. (1997) *Science 276*, 812−816.
47. Boldt, N. J., Donohoe, R. J., Birge, R. R., and Bocian, D. F. (1987) *J. Am. Chem. Soc. 109*, 2284−2298.
48. Heald, R. L., and Cotton, T. M. (1990) *J. Phys. Chem. 94*, 3968−3975.
49. Kim, S., Liang, J., and Barry, B. A. (1997) *Proc. Natl. Acad. Sci. U.S.A. 94*, 14406−14411.
50. Earnest, T. N., Herzfeld, J., and Rothschild, K. J. (1990) *Biophys. J. 58*, 1539−1546.
51. Bernard, M. T., MacDonald, G. M., Nguyen, A. P., Debus, R. J., and Barry, B. A. (1995) *J. Biol. Chem. 270*, 1589−1594.
52. Patzlaff, J. S., Moeller, J. A., Barry, B. A., and Brooker, R. J. (1998) *Biochemistry 37*, 15363−15375.
53. Käss, H., Fromme, P., Witt, H. T., and Lubitz, W. (2001) *J. Phys. Chem. B 105*, 1225−1239.
54. Maeda, A., Susake, J., Yamazaki, Y., Needleman, R., and Lanyi, J. K. (1994) *Biochemistry 33*, 1713−1717.
55. Zundel, G. (2000) *Adv. Chem. Phys. 111*, 1−217.
56. Wang, J., and El-Sayed, M. A. (2001) *Biophys. J. 80*, 961−971.
57. Vassiliev, I. R., Yu, J., Jung, Y. S., Schulz, R., Ganago, A. O., McIntosh, L., and Golbeck, J. H. (1999) *J. Biol. Chem. 274*, 9993−10001.
58. Li, H., Wurrey, C. J., and Thomas, G. J. (1992) *J. Am. Chem. Soc. 114*, 7463−7469.
59. Park, E. S., Andrews, S. S., Ho, R. B., and Boxer, S. G. (1999) *J. Phys. Chem. B 103*, 9813−9817.
60. Hermansson, K. (1993) *Int. J. Quantum Chem. 45*, 747−758.
61. Hermansson, K., and Tepper, H. (1996) *Mol. Phys. 89*, 1291−1299.
62. Phillips, G. N., Teodora, M. L., Li, T., Smith, B., and Olson, J. S. (1999) *J. Phys. Chem. B 103*, 8817−8829.
63. Guex, N., and Peitsch, M. C. (1997) *Electrophoresis 18*, 2714−2723.

BI0110241